Microphone Measurements in Aeroacoustic Installations

Michel ROGER
LMFA, Ecole Centrale de Lyon, University of Lyon
36 Avenue Guy de Collongue, 69134 Ecully cedex
FRANCE

michel.roger@ec-lyon.fr

ABSTRACT

The lecture is dealing with microphone measurements for the investigation of aerodynamic sounds in wind tunnels and similar experimental installations. Because microphones measure static-pressure fluctuations, they can be used either to characterize the sound field or to characterize the flow features it originates from. Both aspects are addressed, as well as technological issues about the mounting of microphones and the separation of the acoustic and aerodynamic motions.

Special thanks. *The author is grateful to E. Salze, P. Souchotte, G. Yakhina and G. Robert from ECL and to M. Jacob from ISAE-SupAero who provided material for the lecture.*

1.0   INTRODUCTION

Microphones are used in aeroacoustics, not only to measure a sound field around or within a flow but also to measure some features of the flow itself. This versatility is explained by the fact that the microphone is sensitive to static-pressure fluctuations, on the one hand, and that these fluctuations in a disturbed flow arise both because of compressibility and because of the inertia variations in a vortical field, on the other hand. In other words the pressure field is of either acoustic or aerodynamic nature. The duality of the measured quantity goes with the versatility of the measuring device, which is in the same time an advantage and a possible drawback. For this reason a clear understanding of the underlying physics is required for a proper interpretation of the measured data. This partially motivated the present lecture organized in three parts. The first part addresses acoustic measurements and the second part aerodynamic measurements. Conventionally the vortical motion of interest in this second part will be referred to as "hydrodynamic" to emphasize its incompressible character, despite the word is questionable in air. The last part is devoted to separation techniques.

2.0   ACOUSTIC MEASUREMENTS

2.1   Basics of Microphones

A microphone is a device that converts local static-pressure fluctuations into an electric signal, with some frequency response and overall sensitivity, generally expressed in mV/Pa. Its directivity, defined as the response as a function of the direction of the incident acoustic waves, is another property of fundamental interest. Various technologies enable this conversion. They are not detailed in this document, more focused on basic principles that must be known for a proper

use of microphones and interpretation of results. Yet the emphasis is on microphones dedicated to physical acoustic measurements.

The first aspect to be considered is that a microphone is an intrusive device when put in a sound field, not rigorously providing an ideal point-measurement. To stress that fact the microphone is considered here as an equivalent membrane or active area excited by the surrounding acoustic pressure. Assume that the active area is a disc of radius r_0 and that a sound wave emitted by a source at very large distance can be described locally as a plane wave of incidence angle θ with respect to the disc plane. Let x and z be the coordinates along the disc diameter aligned with the incident wave and normal to the disc respectively, with origin at the disc center. In the plane (x, z) the incident wave of pressure amplitude A is expressed as

$$p(\mathrm{x}) = A \, e^{i k \cos\theta \, x} e^{i k \sin\theta \, z}$$

where $k = \omega/c_0$ is the acoustic wavenumber. The complementary coordinate y in the disc plane and normal to the direction of the incident wave does not enter the expression. Whatever the technology of the microphone could be, a net force is converted into an electric signal. If the active area is also assumed to integrate the sound pressure like a rigid piston without any additional diffraction effect to produce a measured force p_m, the net result reads

$$p_m = A \int_{-r_0}^{r_0} \int_{-\sqrt{r_0^2-x^2}}^{\sqrt{r_0^2-x^2}} e^{i k \cos\theta \, x} \, dy \, dx = 2\pi A \, r_0^2 \frac{\mathrm{J}_1(kr_0 \cos\theta)}{kr_0 \cos\theta} \qquad (1)$$

where J_1 is the Bessel function of the first kind and of order 1. If $kr_0 \to 0$, which means that the disc is infinitely compact, $p_m \to \pi A \, r_0^2$, or just the incident pressure amplitude times the area of the disc. Microphones used for physical measurements and not for musical needs are usually omnidirectional in this low-frequency regime[1]. But as the disc is not compact anymore the sensitivity of the microphone tends to depend on the incidence angle, because of the dependency $p_m(\theta)$ and other effects associated with the technology of the microphone and the way it is installed. For instance a microphone flush-mounted in a rigid wall may behave differently. Furthermore if the wall is of large extent compared to the acoustic wavelength it is responsible for a reflection of the sound wave, equivalent to adding the image of the incident wave (with angle $-\theta$); the net result is doubling the pressure amplitude at the wall. If other effects are ignored, this "baffle-effect" can be misinterpreted as a doubling of the microphone sensitivity. When a microphone is mounted in a support or a structure of more complicated geometry, its response can be modified by local diffraction effects. This becomes very significant as a large number of microphones are grouped in an array because the supporting structure can be intrusive. Typically supports the cross-section of which is not negligible anymore compared to the wavelengths regenerate diffracted waves that combine with the direct sound. In anechoic open-jet wind tunnels they can be suppressed by a wedge-shaped design of the supports. Finally the real response can also differ from the integral, Eq.(1) because the membrane of the microphone does not respond like a rigid piston. Free-field directivity data for the Bruel & Kjaer microphones are shown in Figure 2-1. The ½" microphone is taken as reference but the results can be transposed

---

[1] Microphones used in music (performances, studios…) are rather designed to have a cardioid directivity. The receptivity is maximum for sounds coming towards the front face of the microphone ($\theta = \pi/2$) and drops in the opposite direction.

to smaller or larger ones because directivity is a matter of Helmholtz number kr_0. Theoretical quarter-space results from Eq.(1) are added as red lines, either considering the total cross-section area as operating (cont. lines) or only 70% of it (dashed lines). The integration effect explains only part of the directivity. Ideally the cross-section of a microphone must be selected as inversely proportional to the characteristic wavelengths $\lambda = 2\pi/k$ to be measured. Furthermore the microphone is better mounted facing the targeted source region, as far as possible.
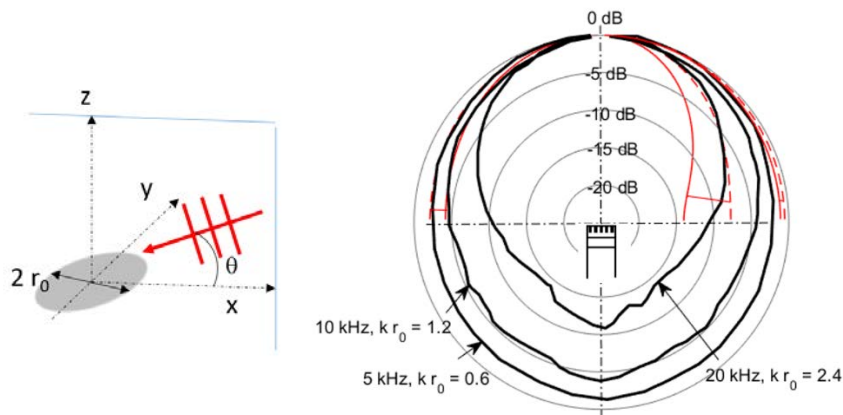

Figure 2-1 - Left: coordinates for Eq.(1). Right: measured directivity diagrams for the B&K ½" microphone (black). Calculations for the full diameter (red cont.) and for 70% diameter (red dashed). 5 kHz and 20 kHz on the right side, 10 kHz on the left side.

Apart from directivity and overall sensitivity considerations, a microphone has a frequency response in amplitude and phase. The amplitude is nearly constant over a more or less extended frequency range and drops beyond some high-frequency (cut-off) that must be also assessed.

2.2   In-Flow Microphones

As far as possible a microphone must be placed away from the flow for various reasons listed below.

1 - As a body in a flow it generates vortical disturbances that are accompanied by local, pseudo-sound pressure fluctuations: this contaminates the acoustic field that is expectedly measured (or the hydrodynamic field if the aim is to characterize the unsteady flow itself). Furthermore the membrane can be stressed and put outside its normal operating range by stagnation-pressure effect.

2 - The microphone is intrusive if embedded in the flow, which possibly generates additional sound sources or unwanted flow distortions.

3 - The microphone in a flow captures pseudo-sound pressure associated with turbulence carried by the flow. This might be unwanted.

Yet in some situations putting a microphone in a flow is unavoidable and special care must be taken for the interpretation of results or for the protection of the microphone. Of course very different issues arise depending on the characteristic Mach number of the flow and depending on what the measurement is aimed at.

First consider the need to measure an acoustic pressure at some point in an undisturbed,

homogeneous flow. In this case there is no pseudo-sound pressure except the one generated by the microphone itself and its support, and the main issue is to protect the microphone. At very low flow speeds this can be achieved by adding a windscreen around the microphone head. Such a device is typically a more or less spherical volume of foam[2] (Figure 2-2-left), therefore it has the drawback of possibly causing attenuation of the sound waves at higher frequencies. The attenuation can be characterized and *a posteriori* corrected. Windscreens are most often used in outdoor measurements or in the quiescent part of an open-jet wind-tunnel installation in the presence of disturbing re-circulations (this reduces pseudo-sound contamination at very low frequencies). However they cannot be used inside the wind-tunnel flow itself as soon as the flow speed exceeds a couple of meters per second. The alternative is to align the microphone with the flow direction and to add a nose cone. The nose cone deviates the mean-flow streamlines and avoids direct stagnation-pressure effect on the membrane. Lateral perforation or an annular strip of porosity allows the local static pressure fluctuations being transmitted to the membrane (Figure 2-2-right). It must be noted that small-scale pseudo-sound pressure fluctuations also develop in the boundary layers of the nose, but their convected nature makes them a secondary issue because they attenuate very fast over a short distance. Nose cones can be used up to indicative flow speeds of 70 m/s but the true limit strongly depends on the level and frequency range of the sound to be measured. The difficulty of properly measuring acoustic waves by placing a microphone in a flow and the associated intrusiveness justify that alternatives are sought. This is why the acoustic measurements are mostly made outside the flow in open-jet wind tunnels or made by flush-mounted or wall-installed microphones in closed wind tunnels. Examples of both strategies will be described in subsequent lectures. Complements are also found in [1].

Figure 2-2 - Windscreens and nose cones for microphones to be used in a flow (from Internet websites).

2.3   Remote Microphones

The idea of using remote (or recessed) microphones has been reported many times in the literature, with very various declinations of the same basic principle: the microphone or any equivalent sensor is located away from the location of the desired measuring point either for protection or space issues. The price to pay is the need for a dedicated calibration procedure aimed at determining the transfer function between the fluctuating pressure at the targeted measuring point and the signal at the microphone. The present document cannot pretend being exhaustive and only indicative examples are cited for conciseness in this section, devoted to acoustic measurements. Other aspects related to aerodynamic measurements will be addressed in section 3.2.

---

[2] It also filters out the effect of turbulence already present in the flow if any.

The first example is the Brüel & Kjaer probe 4182 made of a microphone embedded in a cylindrical body and continued by a thin straight rigid tube of small inner diameter (less than 1mm), similarly to a syringe (Figure 2-3-top). The microphone is in a small box connected to an impedance-matching internal tube wrapped around the preamplifier and the straight tube can have various lengths or be changed for a soft-wall tube. The acoustic plane waves forced inside the tube are attenuated by viscous effect as they propagate to the microphone. The attenuation increases with frequency at a rate that depends on the tube length, according to the data reported in Figure 2-3-bottom[3]. The measurements must be corrected accordingly. The special technology of the probe avoids resonances that would be produced by ending abruptly the head tube on the microphone face.
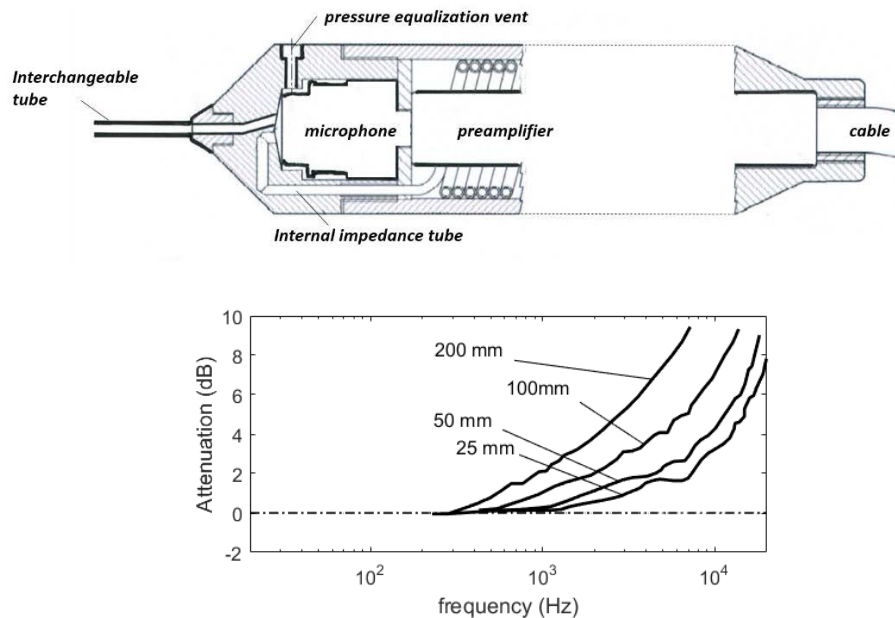

Figure 2-3 - B&K probe microphone 4182. Schematic view and attenuation curves as a function of the length of the head rigid tube. From Website product data.

An alternative is to connect the microphone as a side-branch to the head-tube and to continue the latter over a length very large compared to its diameter. This arrangement is possible if the diameters of the tube and of the microphone do not differ too much. It is technologically very simple but also space-demanding, therefore the continuing tube is often wound with a curvature radius large when compared to the tube cross-section. The acoustic waves are progressively attenuated so that their reflection at the other end of the continuing tube becomes negligible. For this reason the device is referred to as the "semi-infinite waveguide probe". The use of such a probe is reported by Guédel & Farando [2], who made measurements in the exhaust of a turboshaft engine by branching the probe from the inner wall of the exhaust duct. In this case the sound waves at the inner wall are transmitted into the tube. The sound is measured by the side-branch microphone without significant reflection, as long as the connection can be made with no sudden change of the geometry as seen by the acoustic waves. An additional device is

---

[3] Note that this attenuation does not follow the theory introduced later on in section 3.2, which suggests that more complicated phenomena are involved because of the probe design. See product data sheet on B&K website.

needed to cool the initial portion of the side-branch because hot gases are convected in the exhaust duct.

The description of the probe in Figure 2-3-top is the occasion of pointing the importance of the pressure-equalization vent, in this technology and in other devices. For remote microphones connected to a wall over which a mean-pressure gradient develops, for instance because of curvature, the vent must not be obstructed to avoid abnormal constraint of the membrane. This is similar to the effect experienced by the passengers of an aircraft when the pressure inside the cabin varies and that the equalization is not effective through the Eustachian tube in the medium ear.
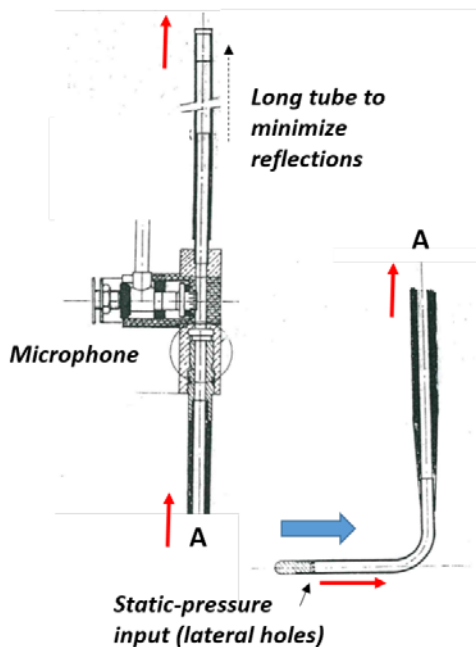

Figure 2-4 - Moving remote-microphone probe for fan-inlet radial scan.

The second example is a specific probe system designed in the seventies by a turbofan manufacturer to explore a radial profile of acoustic pressure in the inlet of a model fan of turbofan engine. In this case the main flow is nearly uniform and unidirectional. This Radial Traversing Probe is made of a single bent tube with its closed end aligned with the flow direction and with its long radial part crossing the duct casing. The probe externally looks like a Pitot tube except that the stagnation pressure is not needed. The local static-pressure fluctuation is captured by lateral perforations in the vicinity of the closed end (see Figure 2-4). Acoustic plane waves are transmitted through the tube with progressive attenuation; they are measured by the side-branch microphone and further propagate along a very long continuation of the tube again aimed at avoiding end reflections, thanks to the cumulated viscous attenuation. By displacing the probe radially a traverse of the sound field in a cross section can be characterized.

The presence of the probe generates a wake that can be a source of spurious noise but, as long as the sound of interest has a very high amplitude at well-identified frequencies such as the blade-passing frequency of a fan and its higher harmonics, this remains compatible with the need. A technical issue with side-branch microphones is that the T-junction can feature sudden cross-section changes that are responsible for a partial reflection of the plane sound waves (see the area marked with the small circle in Figure 2-4). This gives rise to back-and-forth acoustic motion in pure cylindrical parts of the probe, typically between the measuring end and the T-junction, leading to possible resonances. These resonances remain manageable because they are attenuated by viscous effects, as will be discussed in more details in section 3.2 in a similar context, but they make the calibration more challenging. Typically they would be responsible for additional oscillations of the attenuation spectra plotted in Figure 2-3. The design of the junction is a key point. It must be such that the acoustic waves do not see any change in the tube, which in practice is hard to avoid if the tube diameter is significantly smaller than the microphone cross-section. Another aspect is the tube bend between the axial and radial parts, which causes some reflection and transmission. Again, as long as the curvature radius is large enough with respect to the cross-

section of the probe tube, this effect is *a priori* negligible. It can be quantified if needed by invoking the simplified two-dimensional sound-propagation model in a circular bend for which an analytical solution is known [3]. Anyway all undesired effects due to the design of a probe can be corrected *via* the calibration procedure.

Another possible instrumentation for measuring the radial distribution of the sound field in a duct would be using a radial rake of stationary microphones. A similar technique but using Kulite pressure sensors instead of true microphones to get access to the sound field in the exhaust duct of a turbine stage has been reported by Taddei *et al* [4]. In such a case care must be taken of the fact that the microphones or sensors are excited not only by the acoustic waves produced by the aerodynamic interactions but also by the pseudo-sound pressure associated with the wakes. This involves both contamination issues and intrusiveness issues.

Though the aforementioned considerations refer to induct measurements in turbomachines, they can be transposed to any duct configuration, including wind tunnels.

2.4   Flush-Mounted and Recessed Microphones

Picking the acoustic information in a duct directly at the wall, from either flush-mounted microphones or the infinite-waveguide probe described above, is of course a non-intrusive way of investigating the sound. But the consequence is that the measurement is now made beneath the boundary-layer turbulence that generally develops along the wall. This raises the question of the contamination by pseudo-sound pressure associated with that turbulence. The pseudo-sound is not an issue anymore if its level remains much lower than the targeted sound. For instance the tonal fan noise at the blade passing frequency in a turbofan inlet can range between 140 dB and 160 dB, whereas the pseudo-sound pressure at the wall corresponding to the boundary-layer turbulence is of about 80-90 dB (equivalent sound pressure level, ref. 2.10^{-5} Pa). Therefore microphones or sensors able to cope with so high levels and directly flush-mounted at the wall could measure that sound without any need for a decontamination procedure. When compared to the Radial Traversing Probe, the limitation of measuring at the wall is that the inner part of the sound field cannot be directly accessed with a single microphone. But the modal structure of the sound field in a duct, introduced in the lecture by M. Jacob, can be used to reconstruct that field from wall-mounted microphone arrays. The underlying property is that the duct modes are equivalent to oblique elementary waves. Each wave can be identified from its trace at the wall, associated with phase-shifts between signals from various microphones of the array. These modal detection techniques are outside the scope of the present lecture; they are addressed, for instance, in the lecture by M. Åbom.

Anyway the pseudo-sound pressure remains undesirable for acoustic measurements. But advantage can be taken from its rapid attenuation as the microphone is recessed from the wall even by a very short distance, forming a small cavity. The acoustic motion being solution of a wave equation, it propagates also inside the cavity, whereas the pseudo-sound, as solution of a convection equation, drops dramatically inside the cavity (essentially the latter is filled with a stagnant air). This increases the signal-to-noise ratio defined as the acoustic-to-hydrodynamic pressure-amplitude ratio. The recessed-microphone technology has been tested by research teams and is now proposed by microphone suppliers. In practice the wall is continued over the cavity by a layer of porous material in order to minimize aerodynamic disturbances. The layer must be acoustically transparent and ensure a smooth guidance of the flow.
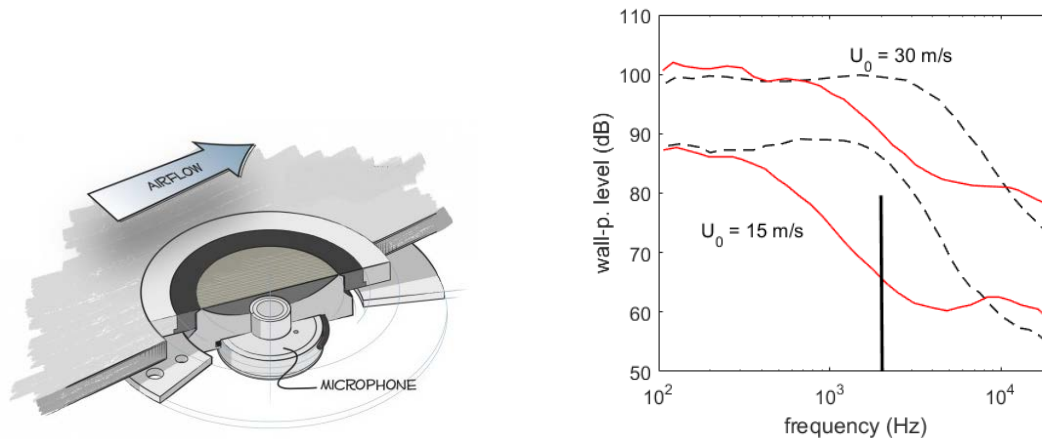
Figure 2-5 - GRAS 67TS Turbulence Screen Kit. Left: technical sketch from GRAS Website. Right: wall-pressure spectra as measured with a flush-mounted microphone and the same microphone with the (from GRAS data sheet).

As an example, data obtained with a recessed-microphone kit designed by GRAS for ¼" microphones are shown in Figure 2-5, to be considered with similar data discussed later on in section 3.1 about aerodynamic measurements. The porous layer is a wire-mesh. What is essentially measured in the test is the wall-pressure spectrum (power spectral density) beneath turbulent boundary layer over a smooth, rigid wall. In absence of external sources, the information is of hydrodynamic nature. Using the recessed microphone with the turbulence screen instead of the flush-mounted microphone, the pressure level is reduced by up to 20 dB. Some high-frequency regeneration of fluctuating pressure is observed, attributed to small-scale turbulence produced on the wire-mesh. This secondary effect is not prejudicial if the sound to be measured is at much lower frequencies. In the present case a sound pressure at the wall of 80 dB as featured by the vertical line at 2 kHz would not be discernable at the flow speed of 15 m/s with a flush-mounted microphone but it would be detected with the recessed microphone.

Another turbulence-subtracting device that can be used in a free stream in the presence of turbulence is the Neise probe [5]. This probe is essentially a long tube with a thin longitudinal slit covered with a cloth. It must be aligned with the flow and is primarily aimed at measuring plane waves propagating downstream; this is explained by the initial need of measuring the sound in an axial-fan test bench. The upstream end of the probe is closed by a nose cone and a microphone is installed at the downstream end. Omitting details that are found in the reference, the principle can be stated as follows. External pressure fluctuations are transmitted inside the tube where they excite sound waves that propagate to the microphone. For downstream plane waves at low Mach numbers the phase differences between the external and internal acoustic fields are small. In contrast the internal sound field induced by external hydrodynamic disturbances suffers from the mismatch between the sound speed and the much lower convection speed, which results in partial cancellation. This strongly reduces the contribution of the hydrodynamic disturbances to the signal measured by the microphone. This device is only mentioned in this section for completeness because its size is often inappropriate. Its use is reported for instance by Frémion *et al* [6].

3.0   HYDRODYNAMIC WALL-PRESSURE MEASUREMENTS

The characterization of wall-pressure fields induced by unsteady wall-bounded flows in a wind tunnel is a topic of interest for various reasons.

1 - The pressure fluctuations force vibrations that can be transmitted or radiate as sound if the wall is not rigid. This is typically what happens as the flow over a car window or over the fuselage of an aircraft generates sound inside the vehicle and contributes to what is referred to as interior noise.

2 - The associated vortical field is a source of aerodynamic noise for the environment by interaction with geometrical singularities if the wall is rigid. This generic mechanism has many declinations such as the trailing-edge noise of a lifting surface, the flow noise around a corner, the vortex-shedding noise of a bluff body, roughness noise and so on.

For both purposes measuring the space-and-time properties of the wall pressure field by means of microphones properly distributed is a way of getting knowledge, not directly about the sound itself but about the sources of the sound. Such an information is of fundamental interest for strategies of noise reduction at source, as well as for the validation of prediction schemes. This section focuses on the transitional or turbulent boundary layers developing over a rigid flat wall or airfoil surface selected as examples, but the same principles or techniques would hold in other geometrical configurations.

3.1   Flush-Mounted and Pinhole-Recessed Microphones

As stated in section 2.3 a possible way of getting access to the acoustic field at a duct wall is using directly flush-mounted microphones. The same mounting is suited for characterizing the hydrodynamic pressure associated with the convected turbulence in the boundary layers of the duct or of any tested aerodynamic body of interest. Various aspects of this choice are shortly addressed in this section.

3.1.1   Effect of Protection Grid

The protection grid of a standard microphone flush-mounted in a wall under grazing flow has a significant effect in the sense that the measurements differ depending on whether the grid is removed or not. In the test cited in this section from Salze *et al* [7], Figure 3-1, the same measurement is repeated with and without the grid in such a way that there is no intrusion in the flow, which means that the membrane is either in the plane of the wall or recessed behind its grid. The boundary layer is turbulent and the wall-pressure is measured at various flow speeds ranging from 30 m/s to 100 m/s by steps of 10 m/s. All power spectral densities (PSD) are plotted in dimensionless form using boundary-layer variables, here the wall shear-stress τ_w and the displacement thickness δ_1, as a function of a Strouhal number based on δ_1. As expected from flow similarity, all spectra collapse when measured by the microphone without its grid. In contrast the PSD has a different and unexpected shape as measured with the grid. Furthermore the spectra are not self-similar anymore at higher frequencies. The first issue is that the recessed membrane is less sensitive to the pseudo-sound information of interest because of the convected character of the latter. The spatial attenuation of the pseudo-sound pressure increases with distance and frequency. This explains the cut-off of the response beyond the Strouhal number of about 1 in the figure. At

higher frequencies pressure fluctuations are probably regenerated in the Strouhal-number range 2-to-10 because the flow over the protection grid produces additional vorticity, as in Figure 2-5. The peak noise at a constant Strouhal number in Figure 3-1-b is caused by the vortex-shedding sound of a Pitot tube placed in the flow.

(a)   (b)
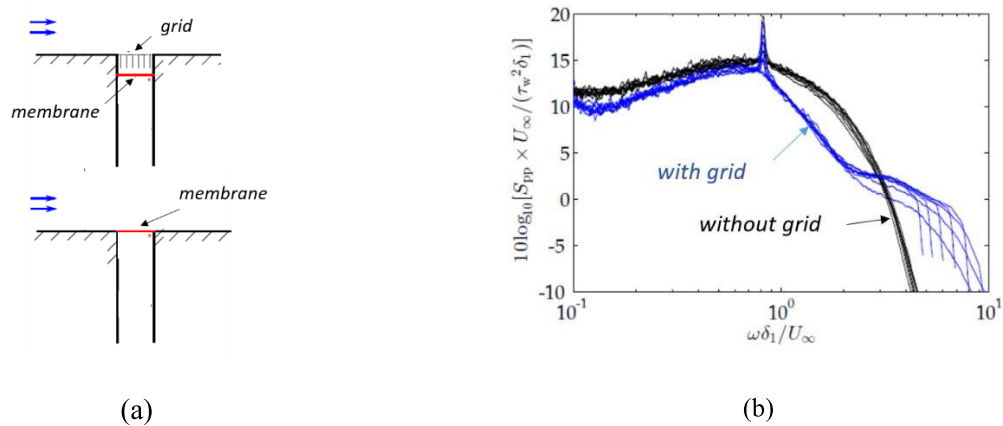
Figure 3-1 - Test of flush-mounted microphones for measurements beneath a turbulent boundary layer. (a): sketch of the mounting technique, grid vs. no-grid. (b): dimensionless wall-pressure spectra for free-stream flow speeds between 30 m/s and 100 m/s. From Salze *et al* [7].

The cut-off of the wall-pressure spectrum is a drawback in this section because the wanted information is the hydrodynamic field but it was an advantage for the acoustic measurements addressed in section 2.4. Indeed the grid filters out part of the pseudo-sound and plays the same role as the porous layer discussed in section 2.4. Recessing the microphone membrane beneath the wall after removing the grid and replacing the grid by a porous layer produces better controlled conditions.

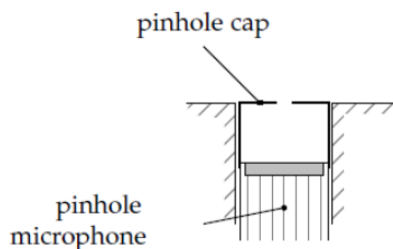### 3.1.2   Microphones under Pinhole

Figure 3-2 - Principle of the pinhole-cavity system for recessed microphones, from Salze *et al* (2014).

Because the grid induces spurious effects and for other issues related to the integration (section 3.4) and to the protection of the microphone, a mounting with a recessed microphone in a small cavity behind a pinhole is a preferable option (Figure 3-2). Indeed, at least at the scale of the hydrodynamic motion, the very small cross-section of the pin-hole will transmit pressure oscillations inside the cavity without significant regeneration of vortical motion. Furthermore it will have a much lower, often negligible, integration. However the pinhole technology modifies the response of the microphone, in particular because the cavity acts as a Helmholtz resonator.

A Helmholtz resonator is a closed volume communicating with the external air by a neck, such that the length and cross-section of the neck are much smaller than the size of the volume. It

is known to have a resonant frequency for which the wavelength is large compared with the size of the volume. The resonance of the pinhole system must be characterized and the response of the microphone corrected accordingly. This will be addressed in the section 3.3 dedicated to calibration procedures. It must be noted that at the size of the pinhole system the prediction of the resonance is made inaccurate by the strong effect of manufacturing details.

Another possible occurrence of Helmholtz resonance will be discussed in section 2.2 below about remote-microphone probes. Details on the Helmholtz resonator and microphone cavities are found in any handbook of acoustics and in the book by Glegg & Devenport [1].

3.2   Remote-Microphone Probes

When wall-pressure measurements must be performed on small-scale mock-ups in a wind tunnel, usually to characterize the convected vortical motion, one of the issues is the available space for the implementation. Any microphone or sensor, even if miniaturized, has a size that can be not compatible with the needs. This typically occurs when the fluctuating wall pressure must be measured close to a sharp trailing edge where the investigated body has a very small thickness, larger than the sensor, or when many sensors must be clustered in order to get multipoint information (cross-spectral analyses). One way of solving the issue is to rely on the Remote-Microphone Probe (RMP) technology already described in section 2.3 for acoustic needs: the microphone is placed outside the mock-up and, of course, outside the flow, and connected to the wall with a pin-hole and a capillary tube. An important feature is that there is no cavity under the pinhole.

One simple way of manufacturing and installing a RMP is to carve grooves on the mock-up surface. Once the capillary tube of a probe is put inside it, the groove is resealed in order to recover the original surface with minimum roughness. Modern rapid-prototyping techniques offer new possibilities, still to be assessed, by programming the capillary directly in the three-dimensional CAD of the mock-up. One difficulty is that the final capillary must have no obstruction and that the material used to manufacture the mockup must not be porous or of variable properties in mid-to-long term with time. The present section only focuses on a classical example of RMP to illustrate the main aspects of the technique, from various investigations made at ECL. Similar devices with very different geometrical parameters have been used by many investigators, for instance amongst others Salze *et al* [8], Fuertes *et al* [9], Moreau *et al* [10], Marsan *et al* [11] and Zawodny *et al* [12].

It must be kept in mind that both acoustic and hydrodynamic motions coincide in aeroacoustics. Depending on the flow regime and on the location along the instrumented surface the local pressure fluctuations can be of either aerodynamic or acoustic dominant nature. For instance if the measuring point is beneath a laminar and stable boundary layer, the measured wall pressure is acoustic and comes from sources located elsewhere. It is *essentially* aerodynamic if the point is in an area of well-developed laminar instabilities or beneath a turbulent boundary layer. Indeed the vortical/hydrodynamic motion is of much larger amplitude than the acoustic motion in most situations, so that the acoustic pressure is often hidden by the hydrodynamic pressure. The interpretation is more ambiguous in transitional, progressively developing boundary layers because the wall-pressure can be of acoustic or hydrodynamic nature depending not only on the location but also on the frequency.

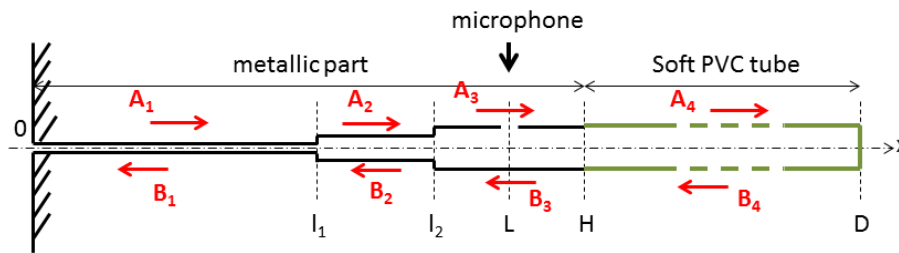### 3.2.1 Typical Remote-Microphone-Probe Technology

Figure 3-3 - Sketch of the Remote-Microphone Probes (RMP) [13] and of the waves generated in each part.

The (RMP) is made of a set of capillary tubes embedded in the tested airfoil mockup, connecting an orifice at the wall to a microphone located outside the wetted part of the mockup. The first capillary tube is perforated laterally at the orifice location. The principle of the RMPs is that wall-pressure fluctuations of any kind (acoustic or "hydrodynamic") at the orifice (0 in Figure 3-3) force sound waves inside the capillary tubes, somewhat like a piston would do. These waves propagate with viscous attenuation and experience multiple reflections at capillary cross-section changes, before being captured by the remote microphone.

(a)

(b)

(c)

Figure 3-4 - Examples of instrumented airfoils. (a): airfoil side with resealed grooves of RMPs [13], measuring points along the chord at mid-span and clustered at trailing-edge (upper edge). Supporting disc and resin block without instrumentation on the right. (b): top view of the resin block showing the connection of the PVC tubes and the laterally branched microphones. (c): RMPs clustered at the tip corner and the trailing edge of an airfoil for the study of tip-gap noise [14]; resin block and microphones not seen, above the upper plate.

The calibration procedure needed to correct both effects is described in section 3.3. It produces a response function or a transfer function between the pressure fluctuations at the probe orifice and at the microphone. A schematic of a RMP is presented in Figure 3-3, where for

simplicity the probe axis is shown normal to the wall instead of parallel (this is not believed to make a significant difference in terms of equivalent inlet impedance). Typical instrumented airfoils are shown in Figure 3-4. The pictures of Figure 3-4-a and -b show the 12-cm chord NACA-0012 airfoil investigated by Yakhina [13] and Figure 3-4-c shows a cambered airfoil of 15-cm chord studied by Grilliat *et al* [14]. The lines of different color visible on the surfaces are the resealed grooves ending at the pinholes.

3.2.2   Analytical Determination of the Transfer Function

As a complement to the experimental calibration procedure, the transfer function of a RMP can be modeled analytically. According to Pierce [15] an acoustic plane wave is exponentially attenuated in a narrow tube (capillary), the modified wavenumber being expressed as

$$K = k + (1 + \mathrm{i})\,\alpha\;; \quad \alpha = \frac{0.0102\,\sqrt{f}}{a\,c_0}$$

where f is the frequency, k the acoustic wavenumber and a is the radius of the capillary cross-section. The imaginary part associated with the factor α accounts for the attenuation (with the present convention of monochromatic waves with time dependence $e^{-\mathrm{i}\omega t}$). As reported by Roger & Pérennès [16] in a study of small-scale high-lift device mockups, this attenuation reaches 25 dB at 20 kHz for narrow tubes of inner diameters of the order of the millimeter, which seems quite large, but the use of microphones for aerodynamic wall-pressure measurements remains reliable above that value.

The probe design of Figure 3-3 involves three capillary tubes of progressively increasing cross-section diameters. The smallest tube of outer diameter 1mm ensures a reasonable access quite close to the trailing edge of narrow airfoils (typically down to 2 mm thickness of the material, thus 1cm from the trailing-edge for the NACA-0012 airfoil of 12 cm chord tested in[13]). The biggest tube is laterally perforated (coordinate L in Figure 3-3) and connected to a side-branched microphone by means of a block of resin in which the tube and the microphone barrel are embedded, in such a way to avoid leakage. The end of the biggest tube is continued by a long soft-wall (PVC) tube aimed at progressively damping the acoustic waves (junction at the coordinate H in Figure 3-3). This PVC tube, of about 2m long, is closed in order to avoid any mean flow in the probe. With this technology, incident sound waves are partially reflected and transmitted at each section discontinuity, but only plane waves are regenerated; therefore two forward and backward-propagating waves result on each side of the discontinuity. The 2 m length is not enough to avoid end reflections at lowest frequencies, typically below 300 Hz in the example. This is why the formulation includes these reflections.

The first equation of the transfer-function model expresses the continuity of acoustic motion at the probe entrance. It relates the amplitudes of the pressure waves inside the capillary of index 1, say A_1 and B_1, to the amplitude of the incident pressure wave A_0 and reads

$$2A_0 = (A_1 + B_1) + \frac{Z_0}{\rho_0 c_0}(A_1 - B_1)$$

It involves the acoustic inlet impedance

$$\frac{Z_0}{\rho_0 c_0} = R_0 + \mathrm{i}\, k\delta_0; \quad R_0 = \frac{k^2 S_0}{2\pi}; \quad \delta_0 = \frac{8\sqrt{S_0}}{3\pi^{3/2}}$$

where S_0 is the orifice area (see [15] or any handbook of general acoustics). This impedance might be the most questionable parameter of the model in view of the various excitations encountered in the presence of flow[4]. Other relations are obtained by imposing the continuity of wave pressure and flow rate on both sides of each cross-section change, according to the generic equations

$$A_j\, \mathrm{e}^{\mathrm{i}K_j \ell_j} + B_j\, \mathrm{e}^{-\mathrm{i}K_j \ell_j} = A_{j+1}\, \mathrm{e}^{\mathrm{i}K_{j+1}\ell_j} + B_{j+1}\, \mathrm{e}^{-\mathrm{i}K_{j+1}\ell_j}$$

$$A_j\, \mathrm{e}^{\mathrm{i}K_j \ell_j} - B_j\, \mathrm{e}^{-\mathrm{i}K_j \ell_j} = \frac{K_{j+1} S_{j+1}}{K_j S_j}\left(A_{j+1}\, \mathrm{e}^{\mathrm{i}K_{j+1}\ell_j} - B_{j+1}\, \mathrm{e}^{-\mathrm{i}K_{j+1}\ell_j}\right)$$

for the pressure and the flow rate respectively, where ℓ_j stands for the coordinate of the j [th] singularity and K_j, S_j for the associated wavenumber and cross-section area. At the end of the PVC tube the residual sound wave is totally reflected with a zero-velocity condition. Solving the system of equations provides the ratio of the complex amplitudes of the pressure waves at the microphone location and at the orifice as a function of frequency [13,16]. The predicted attenuation is plotted in decibels as the dashed black line in Figure 3-8 of the section 3.4.1.

The interest of a model response function is that it can help to interpret dips and humps in a measured response function. It can also be used for a preliminary design of the probes in view of the identified needs. According to previous elements, the effect of longer capillary tubes is to increase the amount of attenuation. Therefore the optimal length is *a priori* the smallest possible one, keeping in mind that all microphones must be kept outside the mock-up, beyond the end-plates used to hold it. But taking benefit of the attenuation is also a way of avoiding saturation. Indeed some microphones initially designed for true acoustic applications can be limited in view of the large amplitude of hydrodynamic pressure fluctuations. As an example Electret microphones with a saturation threshold of about 120 dB were used by Roger & Pérennès [16] to investigate a small-scale mock-up of high-lift devices; this was found suited in view of the final measurements. In contrast, in a study of the rod-airfoil tandem in a flow, Jacob *et al* [17] reported hydrodynamic wall-pressure levels around the leading edge of the airfoil largely exceeding the 120 dB, because of the impingement of the vortices shed by the upstream rod; the same microphones were not usable anymore. For very high levels, classical microphones can be replaced by Kulite sensors.

3.3 Blade-Embedded Microphones

Microphones can also be directly installed inside rotating blades, in which case another challenging point can be the transmission of signals. Many experiments performed in the past used a spinning collector to connect the signals measured by rotating sensors to stationary cables installed in a tube in the continuation of the shaft. This technology must be carefully controlled in order to avoid mechanical imbalance. It can be changed with benefit for more advanced wireless

---

[4] In the analytical response model the pin-hole is considered to have equivalent inlet acoustic impedance, which is *a priori* valid only for acoustic excitation. The same behavior is assumed for hydrodynamic excitation and the inlet impedance is assumed independent of the flow conditions.

transmission techniques using radio waves or infrared sensors. Another alternative, when made possible by the size of the setup, is to fix a recording device directly in the hub of the rotating part so that the whole instrumentation is rotating with the rotor. The low-speed fan application reported by Rozenberg [18] and Rozenberg *et al* [19] is cited here as an example. In this application low-speed fan blades were instrumented with two sets of small-size Knowles microphones (2.6 mm diameter) in order to get access to the wall-pressure statistics in realistic operating conditions for the sake of trailing-edge noise modeling. The microphones, directly supplied with their connecting cables, were inserted in thin metal tubes laterally perforated close to their ends, somehow like the mouth of a flute. The tubes were introduced inside the blades using the same technique as for RMPs, except that the grooves were quite large and the measuring area of the microphones was oriented perpendicular to the wall. Therefore once the grooves were resealed a small cavity remained as illustrated in Figure 3-5. The cavity again acts as a Helmholtz resonator the aperture of which is the pinhole, making careful calibration necessary.
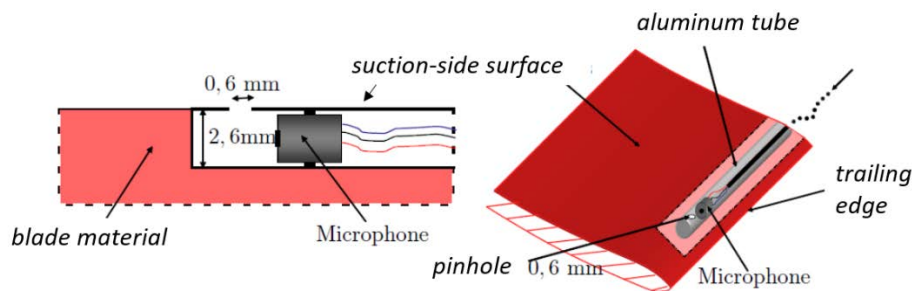

Figure 3-5 - Mounting of small-size Knowles microphones inside a low-speed fan blade, for connection to a ring connector, showing the pinhole and cavity [18].

The instrumentation of the blades is shown in Figure 3-6. The fan hub was large enough to receive the power-supply and the cables of the sensors. Sample results and calibration details are given in the sections 3.4 and 4.
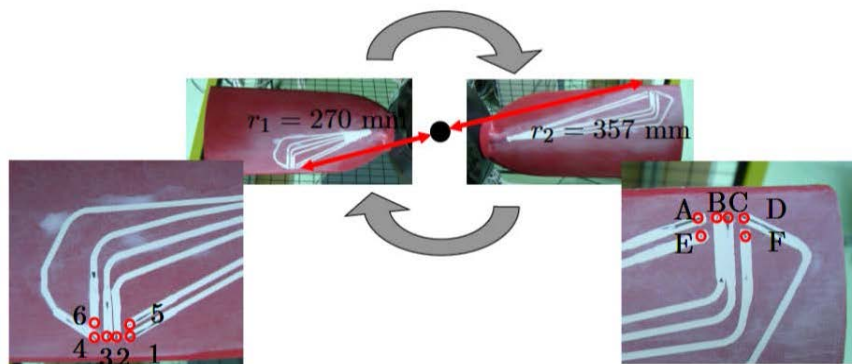

Figure 3-6 - Two-bladed instrumented fan of Rozenberg's experiment, showing the two sets of embedded microphones with their resealed grooves in white, used to characterize the wall-pressure field close to the trailing edge, near the blade mid-span (left) and closer to the tip (right).

3.4 Calibration Procedures

3.4.1 In-Situ Calibration of Remote Microphone Probes

When installed on a wall, a microphone or sensor generally has a modified response with respect to what it would produce in free field. In the case of the RMP described in the previous section, the theoretical transfer function as deduced from the analytical model could be used jointly with a separate measurement of the overall sensitivity of the microphone in free field. Yet additional mounting effects can be suspected. Furthermore the sensibility of the analytical response to variations of the geometrical parameters is an indicator of the consequences of small manufacturing errors. If not properly corrected this variability might cause spurious small-amplitude oscillations in a measured broadband spectrum. Furthermore the model assumptions can be questionable, or at least need to be validated, in some frequency ranges. In other mounting techniques, for instance using a cavity under a pinhole, relying only on theoretical corrections is somewhat questionable. This is why dedicated *in-situ* calibration is required.

Figure 3-7 - Typical device for the calibration of RMPs or similar pin-hole wall-pressure sensors. The tripod end ensures right surface positioning.
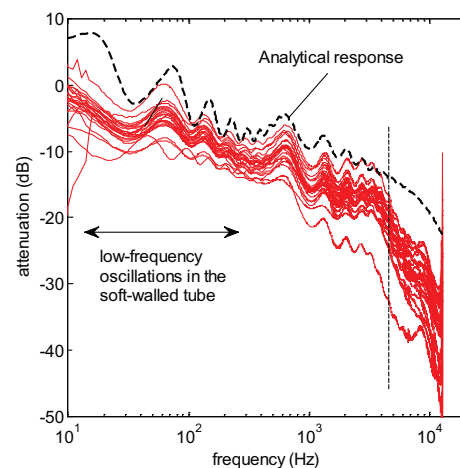

Figure 3-8 - Attenuation spectra as measured by the two-step calibration procedure on the RMPs of the NACA-0012 airfoil in Figure 3-4-a (red plots), and as predicted by the analytical model of section 3.2. Sensitivity ratios not taken into account.

Even if the wall-pressure sensors must be used under a flow, the calibration is often performed with controlled acoustic excitation, which ensures an extended and known frequency content. For this the manufacturing of a calibrator is necessary. The one designed at ECL and used for airfoil-noise studies is shown as example in Figure 3-7. The calibrator is made of a small-size loudspeaker continued by a tube of inner diameter 1 cm. The end of that tube is equipped laterally by a B&K ¼" microphone. Under the excitation by the loudspeaker the latter delivers a signal X_{CAL}. The opening of the tube acts as a piston for most frequencies of interest, typically up to 18 kHz. It is placed successively over the pin-hole of the RMP to be calibrated and over another reference B&K ¼" microphone flush mounted in a rigid flat plate. This second microphone delivers a signal X_{REF}. The loudspeaker is driven by a broadband noise generator. Two transfer functions are acquired: the RMP to calibrator, say X_m/X_{cal}, and the calibrator to reference X_{cal}/X_{ref}. Forming the ratio of both provides the transfer function between the RMP and what a flush-

mounted B&K ¼" would measure, X_m/X_{ref}. Because this calibration is purely acoustic and makes sense for a frequency range in which the diameter of the B&K ¼" microphone remains well compact, it is reliable. Yet the calibrator positioning may not be perfect on some curved parts of airfoil surfaces or close to a trailing edge. Therefore the *in-situ* calibration sometimes requires additional use of a ductile seal. The analytical and measured response functions can be used jointly: the calibration is satisfying when both methods provide similar corrections.
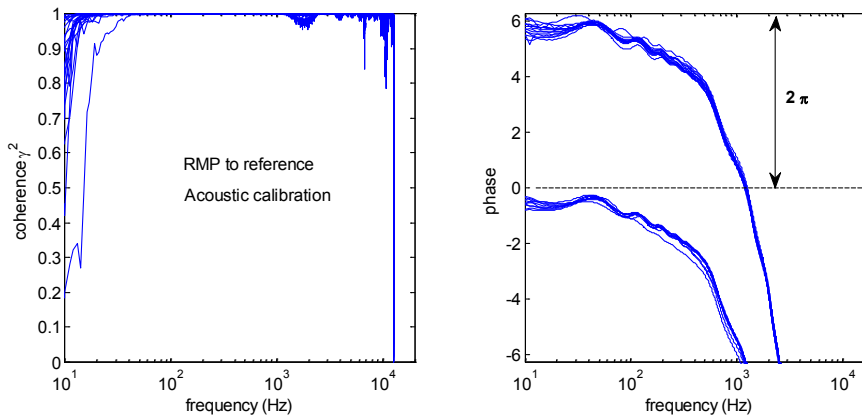

Figure 3-9 - Coherence (left) and phase spectra in radians (right) measured between a set of RMPs and reference microphone.

In the two-step calibration procedure the sensitivity σ_m of the RMP microphone differs from the sensitivity σ_{ref} of the signal of the reference flush-mounted microphone. The sought transfer function is therefore simply expressed by $\left(\sigma_{ref}/\sigma_m\right)X_m/X_{ref}$. Typical direct measurements (uncorrected for sensitivity differences) are plotted in Figures 3-8 & 3-9, from [13]. The coherence and phase plots in Figure 3-9 (left and right respectively) confirm that the RMPs can be used over the entire frequency range without any significant loss of coherence, with a nearly identical and continuous phase variation. These properties ensure that the RMPs can be used with confidence to measure both correlation lengths (from the coherence) and convection speeds (from cross-spectrum phases). This is shortly discussed in section 4.

Theoretical and measured attenuations deviate from each other above 5 kHz in Figure 3-8, where the latter are more pronounced. Furthermore the high-frequency hump measured around 8-9 kHz (or the dip at 6-7 kHz depending on the way of interpreting both) is not found with the theoretical response. These discrepancies can be attributed either to a limitation of the analytical model or to the calibration itself. Anyway a hump at 8-9 kHz has also been observed in the measured spectra (not shown here) with no evidence of physical consistency. The reference 1/4" microphone used for the calibration is flush-mounted with its protection grid removed. This was found to attenuate the response at high frequencies and could explain the aforementioned deviation. Indeed the ¼" microphones of the RMPs still have their protection grids. But the connection with the laterally perforated tube is ensured by means of a pinhole of 0.5 mm diameter in the tube itself and a conical drilling in the resin block. The half apex angle of the cone is 45°, forming a cavity. The latter again acts as an equivalent Helmholtz resonator, the resonant frequency of which can be approximately estimated as

$$f_R = \frac{c_0}{2\pi}\sqrt{\frac{A}{VL_e}} \quad \text{with} \quad V = \frac{\pi(D-d)}{24}(D^2 + Dd + d^2)$$

where A and L_e are the neck cross-section and length (the latter corresponds to the capillary tube thickness), V is the volume of the conical cavity and D and d the diameters of the microphone and of the neck, respectively. The model of section 3.2 should be modified according to the sketch in Figure 3-10 to account for this additional distortion of the transfer function.
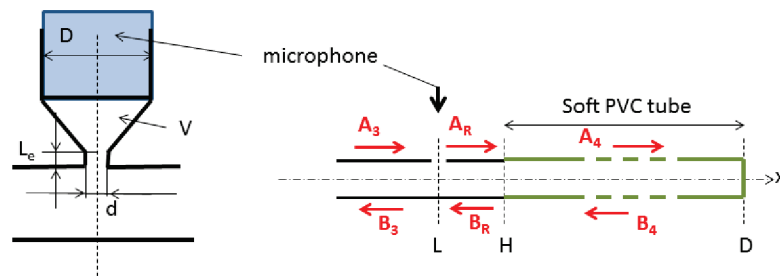

Figure 3-10 - Completed analytical model of RMP. Capillary-microphone junction acting as a Helmholtz resonator.
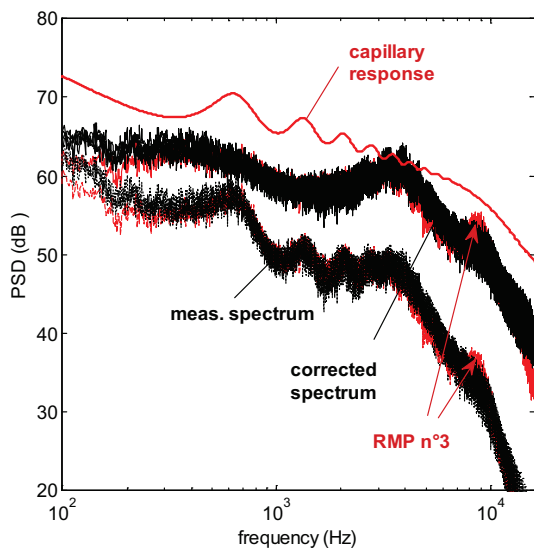

Figure 3-11 - Example of wall-pressure spectrum correction using an analytical model of RMP response function. NACA-0012 airfoil at zero angle of attack, U_0 = 30 m/s. Natural boundary layers with free-stream fine-scale turbulence [13]. Deviation of RMP signal n°3 attributed to manufacturing errors.

A typical example of wall-pressure spectrum correction is shown in Figure 3-11. The configuration is again the instrumented NACA-0012 in Figure 3-4, in a wind-tunnel flow only disturbed by a fine grid put inside the nozzle. The result is a low-level free-stream turbulence for which laminar unstable boundary layers develop on the airfoil without acoustic feedback. In such a case the instabilities cover a limited frequency range, quite different from the broadband content of developed turbulence. The measured spectra are plotted in the figure for a spanwise set of 5 probes at the same chordwise location close to the trailing edge.

They are almost perfectly superimposed because the flow statistics repeats identically along the

spanwise direction, at least once all microphone sensitivities are taken into account. The common measured spectrum exhibits humps and dips that can be either physical or caused by the response of the probe. This is why plotting the theoretical transfer function of the capillary tubes for an excitation of constant amplitude with frequency (red plot in the figure, shifted vertically for convenience) helps identifying the humps and dips of the response due to multiple reflections.

Once the theoretical correction is applied to the measured spectra a much smoother spectral shape is obtained. The first three or four humps were caused by the response of the probes. The corrected spectrum exhibits a broad bump with a dominant frequency around 4 kHz in the present case, which is the true hydrodynamic information corresponding to the instability waves. The minor 'accident' of all spectra around 9 kHz, enhanced on the signal from probe n°3, is attributed to the resonance of the conical cavity. This example illustrates the fact that if not corrected, the probe response can not only produce artificial spectral features but also hide other features of physical interest.

3.4.2 - High-Frequency Calibration of Pinhole-Cavity Probes

Another example of calibration procedure is illustrated in this section in the case of a recessed microphone in a cavity under pinhole, from Salze *et al* [8]. Of course the procedure could be applied as well for any sensor technology.
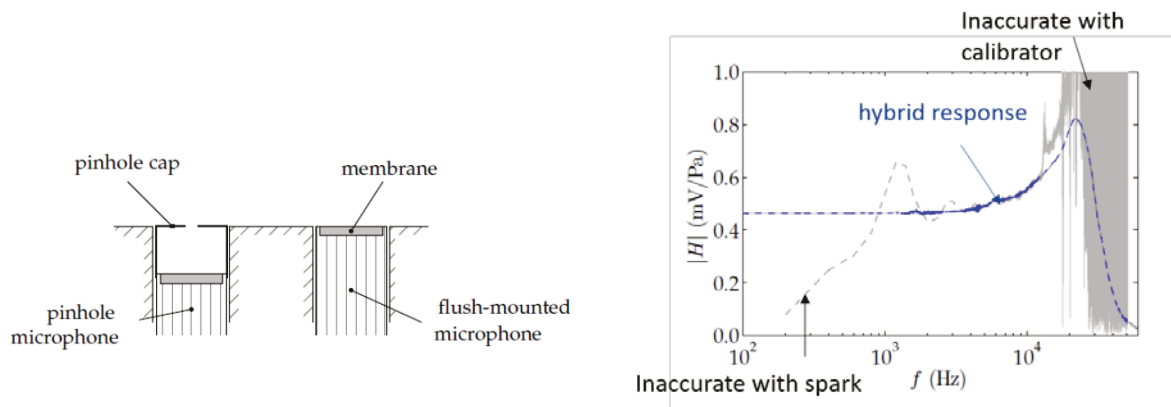

Figure 3-12 - Acoustic calibration of a cavity-under-pinhole microphone by comparison with a flush-mounted microphone with a hybrid method, calibrator plus spark source, from Salze *et al* [8].

The idea is to resort to different techniques for the low-and-middle frequency range and for the high frequency range. Indeed at very high frequencies the calibration with the calibrator shown in Figure 3-7 becomes dramatically inaccurate, whereas it is well suited at lower frequencies. An electric spark generator is used instead, producing high-amplitude impulse shock waves. If the sensor to be calibrated and a reference flush-mounted microphone are placed exactly at the same distance from the spark source, comparing their responses provides the sought response function of the sensor up to several tens of kHz. A typical result is shown in Figure 3-12. The hybrid-reconstructed response is flat at low frequencies up to 3 kHz, then it increases and reaches a peak value before dropping at higher frequencies. The shape of the peak is expected from the Helmholtz resonance and is typical of the pinhole-cavity system [1].

3-4.3 Aerodynamic Calibration

Figure 3-13 illustrates an alternative calibration procedure in which two sensors are installed in a flat plate beneath a turbulent boundary layer. One sensor is the reference and the other one is the sensor to calibrate, namely a flush-mounted B&K ¼" microphone and the embedded Knowles probe of Figure 3-5 respectively in the present case. The main interest is that the sensors are placed in a real configuration of aerodynamic excitation. In practice both are on the same line perpendicular to the flow direction to ensure the homogeneity of the measured fields, unlike what is shown for clarity on the sketch. The possible concern is that the induced wall-pressure might not be strong enough over the whole required frequency range. This is why a small obstacle or step, indicated by the arrow in the figure, is used to generate high-amplitude vortical disturbances. Furthermore the partial cancellation effect resulting from integration over the measuring area of the sensor and/or of the reference microphone must be corrected according to the procedure described in section 3.5.

(a)   (b)
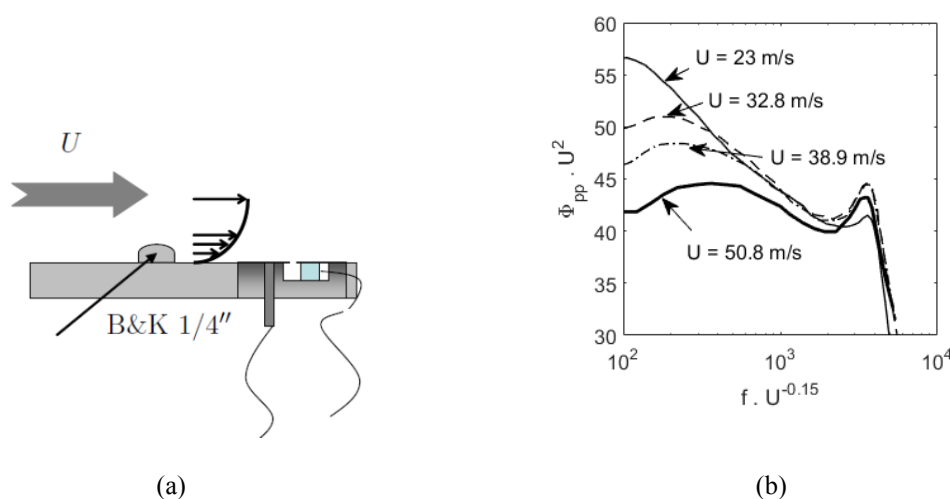
Figure 3-13 - (a): principle of flush-mounted sensor calibration procedure beneath a turbulent boundary layer. In fact both sensor and reference microphone are at the same streamwise location. (b) Reduced wall-pressure spectra, with artificial scaling to point the resonance due to the sensor cavity.

As already found with the hybrid acoustic calibration of the pinhole-cavity device, the response exhibits a hump associated with the Helmholtz resonance of the small cavity. But in the present case the height and center frequency of the hump both depend on the flow speed [18]. Empirical scaling has been attempted in Figure 3-13-b in order to make the humps in the wall-pressure frequency spectra Φ_{pp} collapse at best, which led to the velocity scaling of the resonance with the flow speed to the power 0.15. This stresses that the resonance is neither a pure Helmholtz resonance, because it depends on the flow speed, nor a constant-Strouhal number phenomenon. This also questions the validity of an acoustic calibration procedure for this kind of technology, at least in the present case.

3.4   Integration of Hydrodynamic Wall-Pressure Fluctuations

As already mentioned in section 2.1 the active area of a sensor integrates spatially the measured acoustic pressure. The integration by a flush-mounted sensor of finite measuring area is

even more critical on the hydrodynamic pressure. Indeed the hydrodynamic wavelength $\lambda_H = 2\pi/k_c$ where $k_c = \omega/U_c$ is the hydrodynamic wavenumber is smaller than the acoustic wavelength $\lambda = 2\pi/k$ with $k = \omega/c_0$ by a ratio equal to the convection Mach number $M_c = U_c/c_0$. They strongly differ at low Mach numbers. Let r_0 be the radius of the circular measuring area. The parameter kr_0 is generally small, which means that the sensor area is compact acoustically $(r_0 \ll \lambda)$ and that the measured pressure can be considered as a relevant point value (see again section 2.1). For instance the area of a ¼" microphone corresponds to $kr_0 = 0.06$ at 1kHz (0.6 at 10 kHz). But the lower the convection Mach number the higher $k_c r_0$. At a 0.1 Mach number, $k_c r_0 = 0.6$ at 1kHz so that the same sensor is not compact aerodynamically; there is a significant underestimate of the true pressure level by integration. Correspondingly $k_c r_0$ is 6 for 10 kHz, which lies in the area of large uncertainty for any correction, as discussed below.

The needed correction is generally estimated from Corcos' model [20] based on the assumption of an attached, fully developed turbulent boundary layer on a flat plate under zero streamwise pressure gradient, which is a condition of limited validity. The ratio between the measured power spectral density by the sensor $\Phi_{pp}^m(\omega)$ and the true point-spectrum of the wall pressure, say $\Phi_{pp}(\omega)$, is expressed as

$$\frac{\Phi_{pp}^m}{\Phi_{pp}} = \int_0^{2r_0} \int_0^{2\pi} \Theta(r)\, A(k_c x) B(k_c y)\, e^{-i k_c x}\, r\, dr\, d\theta$$

with

$$\Theta = \frac{2}{\pi^2 r_0^2}\left[acos\left(\frac{r}{2r_0}\right) - \frac{r}{2r_0}\sqrt{1 - \left(\frac{r}{2r_0}\right)^2} \right]$$

$$A(k_c x) = e^{-a\, k_c |x|}; \quad B(k_c y) = e^{-b\, k_c |y|}; \quad x = r\cos\theta; \quad y = r\sin\theta$$

The exponentials forms A and B for the correlations are interpolations of measured streamwise and spanwise coherences. Typical values for the decay rates a and b are 0.11 and 0.714 respectively. But these parameters significantly depend on the streamwise pressure gradient and other experimental conditions, as pointed by many authors. Brooks & Hodgson [21], investigating the boundary layers on a NACA-0012 airfoil of 60 cm chord length, report the values 0.19 and 0.62 at 39 m/s, and the values 0.14 and 0.58 at 70 m/s. Numerical tests are reported in Figure 3-14 where the integration ratio is plotted as a function of $k_c r_0$ both in linear and logarithmic scales. It is also worth noting that Corcos' analysis assumes some important statistical properties leading to the separation and shape of the functions A and B that could be questioned in some flows. Starting from numerical simulations, Singer [22,23] suggested more general expressions. As an example the effect of a different shape for B is also plotted in the figure as the dashed red line; the alternative expression reads

$$B(k_c y) = \frac{C_s^2}{C_s^2 + (k_c y)^2}; \quad C_s = 0.9$$

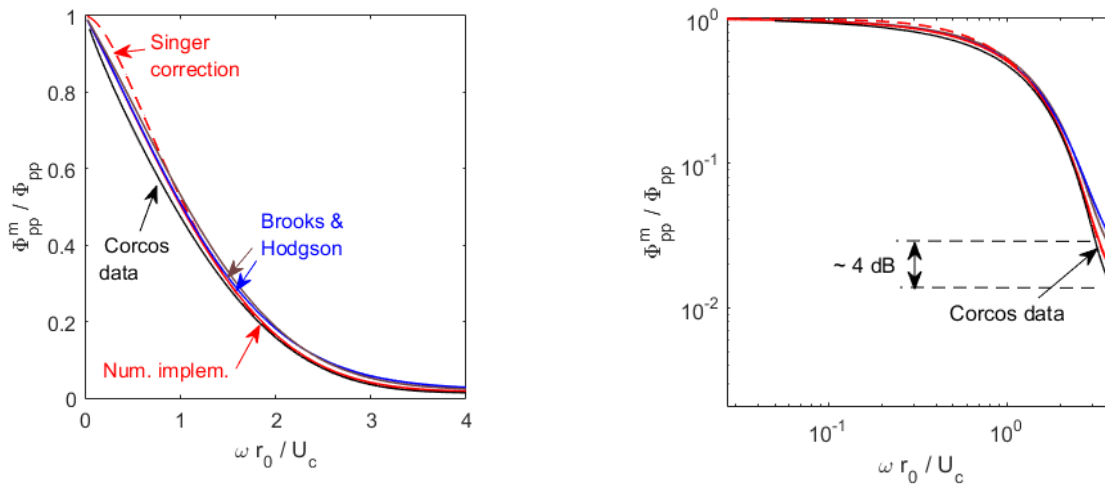and means that the exponential decay might not be the best fit.

Figure 3-14 - Estimation of the integration effect on wall-pressure spectral measurements by circular measuring areas. Corcos' model for flat-plate and airfoil boundary-layer parameters and Singer's correction of Corcos' model [20,22,23]. Linear (left) and logarithmic (right) scales.

Differences in Figure 3-14 are not dramatic but the right plot suggests that the correction could be inaccurate by a couple of equivalent decibels in many cases at higher frequencies because of the scatter of model data. Indeed the integration effect depends on the unknown statistical properties of the wall-pressure field to be measured, which makes the correction exercise implicit.

Surprisingly the integration can be significant at low speed even with a sensor pinhole, the diameter of which is half a millimeter. If the convection speed is 10 m/s, for instance, $k_c r_0$ is 0.63 at 4 kHz. Complements about this important integration effect are found in the handbook by Blake [24].

4.0 APPLICATIONS AND SEPARATION TECHNIQUES

The duality of pressure fluctuations, crucial for instrumented walls in a flow, possibly makes the hydrodynamic pressure or pseudo-sound a spurious information when addressing the acoustic pressure and *vice versa*. Therefore separation techniques able to discriminate both have a major interest. Some of them are rapidly outlined in this section in connection with basic post-processing techniques of microphone signals. The latter depend on what the experiment is aimed at, so that specific applications are considered as examples, focused on airfoil-noise studies.

4.1 Characterization of Trailing-Edge Noise Sources

Trailing-edge noise of airfoils considered as generic lifting surfaces used in many applications, such as blades and vanes of turbomachinery stages, high-lift devices and son on, is one of the commonly investigated mechanisms in wind tunnels. This noise is due to the reorganization and partial conversion of the vortical disturbances carried in the boundary-layers as sound as they are convected past the trailing edge. Existing models in the literature state that the statistics of the radiated sound field can be related to the statistics of the hydrodynamic wall-

pressure closely upstream of the trailing edge. The former is the effect and the latter is the cause. Therefore the instrumentation of an airfoil involves clustered wall-pressure sensors at the trailing edge. The needed statistical parameters are the local wall-pressure power spectral density (PSD) and the associated spanwise correlation length, because the far-field pressure PSD can be expressed as proportional to the product of both. Furthermore the wall-pressure close to the trailing edge must be a homogeneous random field for the model and the associated instrumentation be relevant, for two reasons.

1 - Chordwise homogeneity makes that the precise location of the sensors and their exact distance to the edge do not matter. Because no sensor can be installed in the very vicinity of an airfoil with a sharp trailing edge in view of the lack of space, this property is essential for the validity of the measurements. It is also worth noting that measuring too close to the trailing-edge would provide a combined information coupling the incident hydrodynamic pressure and its contamination by the near-field acoustic pressure from the trailing-edge sources. Therefore is could be more difficult to interpret.

2 - Spanwise homogeneity is expected for extruded bodies in a wind-tunnel flow. It allows reducing the number of sensors required to instrument a long-span body.

For lifting surfaces and curved surfaces, the chordwise/streamwise homogeneity is questionable because of a non-zero pressure gradient and of the natural growth of a boundary layer. Yet it is assumed in many airfoil trailing-edge noise validation studies, which could be detrimental to the success of comparing predictions to measurements. The need for information is precisely denser where it is more difficult to put sensors. The minimum effort is to design two arrays of sensors along the chordwise and spanwise directions within a sufficiently small portion of the chord in the aft part of the airfoil. This is why the choice of the probe locations is a very challenging task, especially on small mock-ups.

Quite logically, trailing-edge noise can be modeled ignoring the chordwise/streamwise correlation length because the vortical field in the boundary layers enters the problem only as it is interacting with the edge. In other studies, for instance measuring the pressure field over an extended surface for characterizing the excitation of structures in a flow, a two-dimensional correlation would be needed.

4.1.1 Determination of Spanwise Correlation Lengths

An important input data for trailing-edge noise predictions is the spanwise correlation length of the hydrodynamic wall-pressure just upstream of the trailing edge, deduced from spanwise coherence measurements between pairs of wall-pressure sensors[5]. The coherence is a normalized quantity obtained from the cross-spectral density of two signals. It gives an indication of the degree of linear relationship between the two signals. The definition is

$$\gamma_{1,2}^2(\omega) = \frac{|S_{1,2}(\omega)|^2}{S_{1,1}(\omega)\, S_{2,2}(\omega)}$$

where $S_{1,2}(\omega)$ is the cross-spectral density and $S_{j,j}(\omega)$ is the (auto-)spectral density of the signal numbered j. $S_{1,2}(\omega)$ is expressed as $p_1(\omega)\, p_2^*(\omega)$ in terms of the Fourier transforms of the

---

[5] The correlation length is also of interest for other spanwise-distributed sources, such as those of the turbulence-impingement noise of an airfoil, of the vortex-shedding noise of an extended bluff body or of a cylinder of large aspect ratio in a flow, and so on. It is an indicator of their efficiency and is usually involved in prediction models.

pressure signals, * standing for the complex conjugate. The coherence varies between 0 and 1, 0 meaning that there is no linear relationship at all. In the present case the two signals are delivered by microphones or probes at the same streamwise/chordwise location on a mock-up but with a varied spanwise separation η_2. The correlation length is defined as a function of frequency by the integral of the square-root of the coherence over all values of the separation:

$$\ell_2(\omega) = 2 \int_0^\infty \sqrt{\gamma_{1,2}^2(\omega,\eta_2)} \, d\eta_2$$

(see for instance [25] for more details). In practice only a limited number of values of the separation η_2 can be obtained in an experiment. It is understood that they are fitted by some theoretical law to allow the computation of the integral, for instance an exponential decay of $\gamma_{1,2}^2$ with η_2. In order to maximize the number of values for the separation with a given array, the spanwise distribution of wall-pressure sensors must be optimized, with uneven spacing.

An example from the same low-speed fan as described in Figure 3-6 is shown in Figure 4-1, where coherence spectra are plotted with a logarithmic frequency scale. Unlike what could happen with a single airfoil held between end-plates in an open-jet wind tunnel, some of the spurious or background noise sources are avoided in this case because there is no additional surface in the flow. The decrease of coherence in the low-frequency range is clearly highlighted and it is found that a log-normal law is a model compatible with the data. The same shape is therefore expected for the spanwise correlation length [26]. The well-known Corcos' model for turbulent boundary layers over a flat plate states that correlation is inversely proportional to frequency. This is relevant in the middle-and-high frequency range but obviously deviates from the physics at very low frequencies. The latter can be not accessible in many wind-tunnels because of background-noise issues. Other data fits for the correlation can be produced using Efimtsov's model [27,8].

The coherence clearly decreases with increasing separation in Figure 4-1, which indicates that the measured information is of hydrodynamic nature. Therefore the measurements are representative of the sources of the sound. Indeed, even though perfectly coherent, the acoustic pressure is so small at the probe locations that it is overwhelmed by the hydrodynamic pressure.
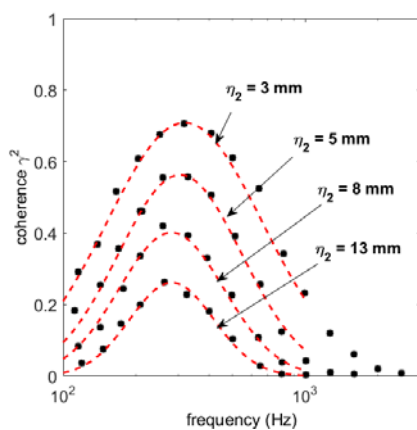

Figure 4-1- Smoothed coherence spectra (black dots) measured by the spanwise set of 4 probes in Figure 3-6 (4 values of the separation of pairs of probes). The red dashed lines stand for an empirical log-normal model [26].

4.1.2 Determination of Convection Speeds

The cross-spectral density $S_{1,2}(\omega)$ between wall-pressure signals measured at two different streamwise probe locations and the same spanwise location is also used to characterize not only the correlation length but also the local convective properties of the wall-pressure field. But the result has to be carefully analyzed in view of the relatively small coherence of the turbulent motion in a boundary layer. Let η_1 be a small separation between two streamwise sensors beneath a boundary layer and a vortical field assumed frozen convected at some speed U_c over the two sensors. Any Fourier component of the vortical field has the form $e^{-i(\omega t - y_1/U_c)}$ where y_1 stands for the streamwise coordinate. The instantaneous phase shift between the sensors reads $\phi = (\omega/U_c)\eta_1$. In the case of a broadband wall-pressure spectrum induced by turbulence the phase of the cross-spectrum expectedly exhibits a linear variation with frequency, at least over some frequency range. The slope of the measured phase variation provides an estimate of an averaged convection speed as

$$U_c = \frac{\Delta\omega}{\Delta\phi}\,\eta_1$$

All reported data point that this estimate depends on the separation η_1. This can be crudely explained as follows. The wall-pressure results from integration of surrounding velocity fluctuations in a finite volume around the measuring point. Small eddies closer to the wall and convected at lower speed can combine with larger eddies convected faster and farther away from the wall to produce pressure fluctuations at the same frequency. Now larger eddies remain coherent over a larger distance. They could be the only coherent ones for some separation η_1 whereas smaller eddies would also be for a smaller η_1. This is why, as a statistical parameter, the convection speed must be estimated from various separations before concluding to its robustness.
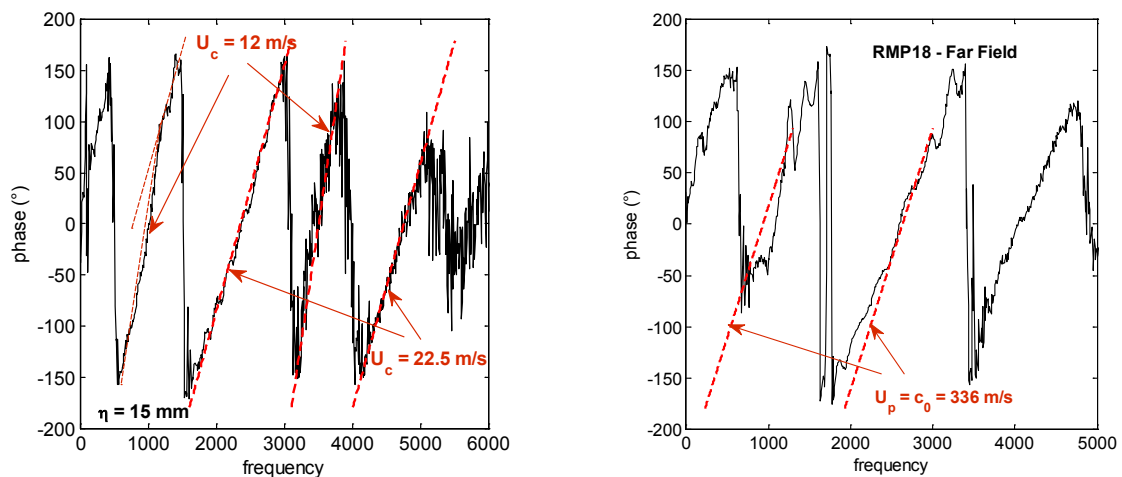

Figure 4-2 - Phase distributions of cross-spectra in an experimental investigation of a transitional airfoil (tonal trailing-edge noise configuration). NACA-0012 airfoil, flow speed 30 m/s, zero angle of attack. ECL data [13]. Left: between 2 streamwise sensors close to the trailing-edge. Right: between a sensor near the trailing-edge and the far-field microphone.

Typical measurements performed on the transitional airfoil investigated by Yakhina [13]

are shown in Figure 4-2. This test case differs from many airfoil-noise studies by the fact that the boundary layers are laminar and unstable, leading to the emission of tonal trailing-edge noise. Indeed the instabilities develop in a limited frequency range within which discrete frequencies are amplified by acoustic feedback. The left plot corresponds to two streamwise sensors close to the trailing-edge. The phase spectrum exhibits two different slopes depending on the frequency range, which seems surprising. The corresponding convection speeds are 22.5 m/s and 12 m/s for a free-stream velocity of 30 m/s. The value 22.5 m/s ($U_c/U_0 = 0.75$) is first found in the range from 1200Hz to 3200 Hz which is precisely the main hump of large coherence in the spectrum associated with the instabilities (not shown). It repeats in the range 3.8kHz-5kHz that corresponds to a secondary hump. The lower convection speed of 12 m/s ($U_c/U_0 = 0.4$) is found between the two aforementioned humps and below 1200Hz, so outside the domain of the instabilities.

In this complicated case different values are found because different physical phenomena take place in various frequency ranges. In broadband trailing-edge noise studies for typical turbulent boundary layers the convection speeds are more homogeneous and U_c/U_0 varies between 0.65 and 0.8. The right-plot cross-spectrum phase in Figure 4-2 is calculated for the far-field microphone and a wall-pressure sensor near the trailing edge of the airfoil. The result is expected from the cause-to-effect relationship between the sound and its source. Indeed the slope of the diagram is compatible with a phase speed U_p equal to the propagation speed 336 m/s as deduced from the airfoil-to-microphone distance of 1.5 m in the experiment.

Another example of the use of clustered wall-pressure sensors is reported in Figure 4-3 [28,29]. The investigated airfoil is a NACA-0012 of quite large size, which allowed producing a well-resolved time-space correlation in terms of streamwise separation and time delay between sensor pairs. Enough resolution is achieved, not only for a reliable assessment of the iso-contours of the correlation but also for the determination of a statistical convection speed, deduced from the inclination of the pattern in the time and space axes. For small separations the convection speed is deduced as 9 m/s, thus the ratio U_c/U_0 is about 0.6 whereas for larger separations the ratio is about 0.85. This confirms the aforementioned effect of separation.
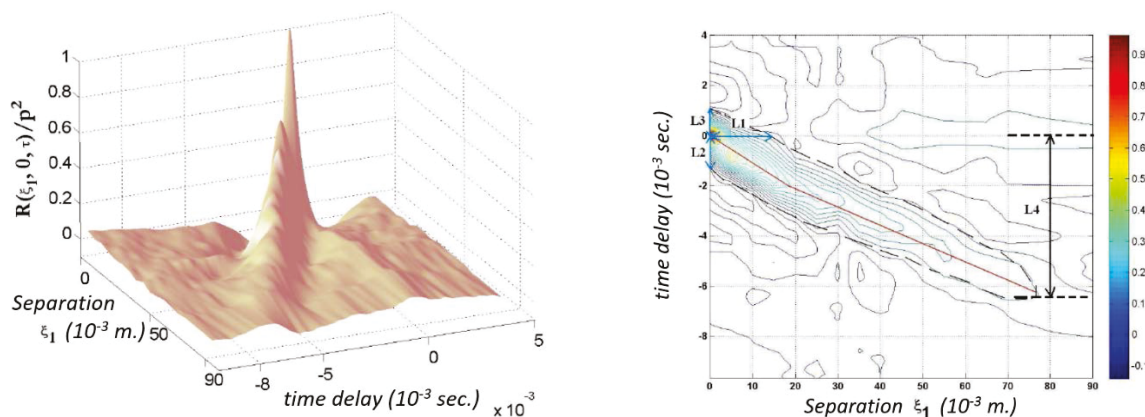

Figure 4-3 - Time-space wall-pressure correlation results from an array of wall-mounted microphones in a NACA-0012 mockup [28,29]. Flow speed 15 m/s.

4-2 Separation Techniques

In many configurations the duality of the static-pressure fluctuations makes their analysis ambiguous. Several techniques are available for the separation of the acoustic and hydrodynamic fields, all based on their different physical features, reminded here from the introductory lecture by M. Jacob.

1 - As a linear solution of the wave equation, the acoustic field is of very small amplitude and almost perfectly coherent, whereas the vortical motion associated with turbulence is known to be of larger amplitude but poorly coherent. Though vortical in essence, laminar boundary-layer instabilities are more coherent, which possible motivates a re-examination of this difference.

2 - The vortical motion is convected, so that its phase speed is the local flow speed or a portion of it. In contrast the acoustic pressure propagates at the sound speed combined with the local flow speed. This property can be used to identify the character of the fluctuating pressure.

4.2.1 Acoustic decontamination

In this sub-section a technique is described to suppress the acoustic contamination of a targeted hydrodynamic field. The next one will be dedicated to the complementary problem of extracting the acoustic pressure of interest from measurements contaminated by hydrodynamic disturbances. This last part is only aimed at introducing a wide area of advanced processing techniques. It is considered as a necessary minimum background for adequate determination of the number and locations of microphones in an experiment.

When microphones are used in a closed wind tunnel to characterize hydrodynamic pressure fields beneath the boundary layers developing on the walls of the wind tunnel itself, the background acoustic field possibly contaminates the measurements and must be subtracted. In an acoustically treated wind tunnel, this is only a matter of concern at very low frequencies for which only the plane-wave duct mode[6] propagates, because these frequencies are hardly absorbed. The homogeneity of the plane-wave in any cross-section provides a very simple way of suppressing the acoustic contribution from the measured spectrum. Indeed consider two microphones in the same cross-section of the duct but sufficiently apart from each other so that the pseudo-sound parts of the signals are not correlated to each other. Because the acoustic part is perfectly in-phase it is suppressed by just making the difference of the two signals. In contrast the two remaining pseudo-sound contributions are identical if the wall-pressure field is homogeneous, which is accounted for by a subtraction of 3 dB. An example taken from the project ENABLE is illustrated in Figure 4-4 [30]. The project was aimed at measuring the wall-pressure field beneath a turbulent boundary layer and microphones where flush mounted on one wall of a duct of rectangular cross-section directly fixed to the nozzle of a wind tunnel. The difference spectrum and a raw spectrum from one of the microphones are plotted. The latter (in black) exhibits a high-amplitude low-frequency part that is absent in the former (in red) and that obviously deviates from expectations. As a result the difference spectrum is relevant over the whole frequency range. It is worth noting that at higher frequencies (beyond the cut-off frequency of the first transverse mode) this procedure would not work; but the installation does not involve high-level acoustic waves at such frequencies thanks to the acoustic treatment in the present case. An alternative way of achieving the same subtraction is described in the following sub-section.

---

[6] Strictly speaking the plane wave is not a solution in a duct with liners. The word is used here to refer to the fundamental mode characterized by the absence of nodes in the cross-section, equivalent to constant-phase field variables.
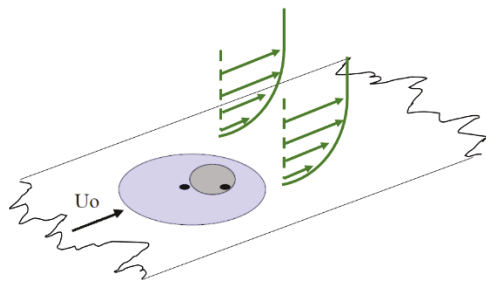
Bottom duct wall with the double-disc device and two flush-mounted microphones (or pinholes)
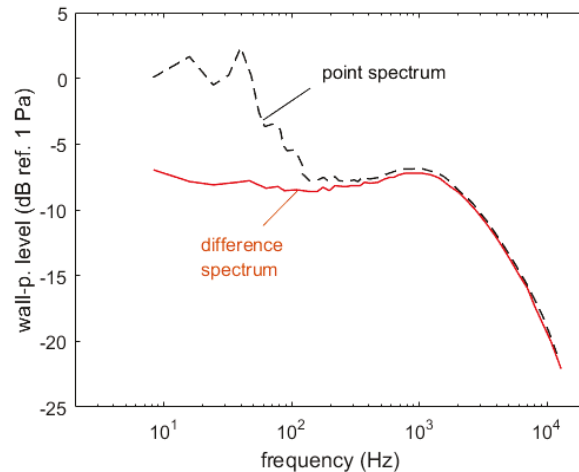
Figure 4-4 - Acoustic decontamination of a hydrodynamic wall-pressure spectrum by the difference-spectrum method. From ENABLE research project [30].

Figure 4-4 is also the occasion of mentioning a clever system in which a large number of separations and orientations of a pair of measuring points can be generated only using two sensors, for the sake of accessing the frequency-wavenumber spectrum of wall pressure fluctuations. A smaller disc is inserted in a larger one, both of them rotating at any angular position, with two pinholes and recessed or remote microphones close to the edge of the smaller disc.

4.2.2   Hydrodynamic/Acoustic Separation by Coherence Measurements

Cleaning microphone signals from the pseudo-sound to extract the acoustic pressure is one of the challenging tasks encountered in aeroacoustic measurements because the latter can be of a much lower amplitude than the former. The coherence can be used to discriminate the two kinds of motion, keeping in mind that it is nothing but a way of assessing the degree of linear relationship between two signals. The latter can be cause-to-effect relationship or linearity between two effects of the same cause, and so on. Coherence can be also used to separate the contributions of various source regions in a total sound field. The background for advances coherence techniques is found in the book by Bendat & Piersol [31]. Non-exhaustive, illustrative examples, as well as a list of references, are given by Frémion *et al* [6] dealing with the identification of the sources of high-speed train noise, and by Guédel & Farando [2] dealing with the separation of core-noise source in a turboshaft engine. Both applications differ by the fact that external and internal instrumentations are described, respectively. The first one is cited also here because it reports the use of a Neise probe.

The basis for the decontamination/separation is the calculation of the Coherent Output Power (COP). For two signals numbered 1 and 2, the COP is defined as

$$\text{COP}_{1,2} = \gamma_{1,2}^2(\omega)\, S_{2,2}(\omega)$$

and the index 1 refers to a detection signal whereas the index 2 refers to the output signal. In

aeroacoustic applications the measured sound often results from various sources. The detection signal is delivered by a pressure probe in one of the source regions where vortical disturbances develop and the output is the signal delivered by a microphone in the acoustic field, possibly in a flow. Both the detection and output signals are contaminated by undesired "noise" in the sense of signal processing, which means that each wanted information is polluted. It can be shown that

$$\text{COP}_{1,2} = \frac{S_{yy}(\omega)}{1 + NSR(\omega)}$$

where $S_{yy}(\omega)$ is the wanted cleaned output and $NSR(\omega) = S_{n,n}(\omega)/S_{xx}(\omega)$ the noise-to-signal ratio associated with the source signal, introducing the FFT of the pressure signals as

$$p_1(\omega) = p_x(\omega) + p_n(\omega) \; ; \quad p_2(\omega) = p_y(\omega) + p_m(\omega)$$

If $p_x(\omega)$ refers to what is measured by a wall-mounted microphone in the source region of some aerodynamic noise mechanism, $p_n(\omega)$ denotes the associated spurious information, of any kind (pseudo-sound or sound form other sources not correlated with the source of interest). In the same way if $p_y(\omega)$ stands for the sought acoustic pressure $p_m(\omega)$ is some contamination, for instance by unavoidable pseudo-sound. It is assumed here that the noisy contributions are neither correlated with each other nor with the quantities of interest. Furthermore, of course, there is a linear cause-to-effect relationship between $p_x(\omega)$ and $p_y(\omega)$. This is what the technique is aimed at highlighting. If $NSR(\omega)$ is small the COP directly provides an estimate of $S_{yy}(\omega)$.

For a better estimate three microphones must be used (see details in the references), two of which must be representative of the same source region. In this case the signals $p_{x1}(\omega)$ and $p_{x2}(\omega)$ must be linearly related, which is ensured if they correspond to the same source. The actual contribution of the source to the sound is estimated as

$$\text{COP}_{1-2,3} = \sqrt{\frac{\gamma_{1,3}^2(\omega)\gamma_{2,3}^2(\omega)}{\gamma_{1,2}^2(\omega)}\,S_{3,3}(\omega)}$$

where the index 3 now refers to the output and the indices 1 and 2 to the source signals.

Based on this idea, Frémion *et al* [6] installed several microphones dedicated to aerodynamic measurements close to various expected source regions of a junction between two carriages of a high-speed train. The source regions were areas around the bogie and in the inter-carriage cavity. In addition, Neise probes were fixed to the train wall at some lateral distance in the external flow for the acoustic measurements. This allowed discriminating some areas as dominant contributors for various frequency ranges. Guédel & Farando partially succeeded in separating internal sources of the exhaust noise of a turboshaft engine[7].

Going back to the case depicted in Figure 4-4, the COP can also be applied to the doublet of wall-pressure microphones if they are sufficiently apart from each other for the hydrodynamic parts of their signals be uncorrelated. It directly produces the acoustic PSD. The hydrodynamic PSD is then obtained by subtracting the latter from the total PSD of one sensor.

---

[7] A similar technique is currently used to separate the sources of turbofan engines.

Comments can be made with respect to the localized or distributed character of aerodynamic noise sources. If one source sensor only is placed in the very vicinity of a localized source, for instance a corner source on a mock-up, its signal will have a significant coherence with the far-field microphone. In contrast if it is placed within an extended source region such as that of the broadband trailing-edge noise of an airfoil, the coherence will be small because the spanwise extent of the source region is much larger than the spanwise correlation length. The source sensor will be only representative of a small portion of the sources. However, in the special case of the tonal trailing-edge noise of airfoils caused by laminar instabilities reinforced by acoustic feedback it has been found that the spanwise coherence of the source region is much larger [13]. In this case the same sensor on the same airfoil will have a very coherent signal with the far-field microphone. This is why the instrumentation of aerodynamic bodies tested in a wind tunnel must be carefully defined, and why enough microphones or sensors must be used in order to properly characterize the correlation lengths. In many cases, *a priori* knowledge or assumption about the sources to be characterized is involved.

5.0   CONCLUDING REMARKS

Many aspects of the use of microphones in wind tunnels have been shortly described in this lecture. Some of them are only mentioned to encourage the reader to more deeply examine the literature. Furthermore the technology of unsteady pressure measurements is improved continuously in the community. In particular important complements could be added on recently developed 'numerical' microphones, for which the functions of pre-amplifier and the connections are strongly reduced in size, or integrated pressure sensors. Such technological advances redefine the constraints to cope with in the design of instrumented experimental setups. Special paintings sensitive to pressure fluctuations also exist. All these exploratory topics are beyond the scope of the lecture.

The acoustic/hydrodynamic duality of pressure fluctuations was the recurrent theme of the lecture, considered as the most important feature. This duality has motivated many efforts to develop and enhance the capabilities of separation and decontamination procedures. The objective was to provide a minimum knowledge of the processing techniques to point how much the installation of microphones is critical to ensure relevant results. The wide range of techniques would deserve another dedicated lecture. Up to that point addressing the separation of the acoustic and hydrodynamic motions reveals itself a fascinating topic and in the same time is equivalent to opening Pandora's Box.

6.0   REFERENCES

[1] S. Glegg & W. Devenport, *Aeroacoustics of Low Mach Number Flows – Fundamentals, analysis and measurement*, Academic Press 2017.

[2] A. Guédel & A. Farrando, *Experimental Study of Turboshaft Engine Core Noise*, J. of Aircraft, 23(10), 1986.

[3] P.E. Krasnushkin, *On waves in curved tubes*, Uch. Zap. Mosk. Gos. Univ. 75 Bk 2 Pt 2 927, 1945.

[4] F. Taddei, C. Cinelli, M. De Lucia & C. Schipani, Experimental investigation of low pressure turbine noise: Radial mode analysis for swirling flows, 12th ISROMAC, paper 314, Honolulu HA, 2009.

[5] W. Neise, *Theoretical and experimental investigations of microphone probes for sound measurements in turbulent flows*, J. Sound Vib. 39(3), 371-400, 1975.

[6] N. Frémion, N. Vincent, M. Jacob, G. Robert & A. Louisot, *aerodynamic noise radiated by the intercoach spacing and the bogie of a high-speed train*, J. Sound & Vib. 231 (3), 577-93, 2000.

[7] E. Salze, C. Bailly, P. Souchotte, E. Jondeau & D. Juvé, *Mesures de pression pariétale instationnaire en soufflerie*, 5ème journée IMAT - IMagerie Acoustique et ses Techniques, Massy, 2015.

[8] E. Salze, C. Bailly, O. Marsden, E. Jondeau & D. Juvé, *An experimental characterisation of wall pressure wavevector-frequency spectra in the presence of pressure gradients*, Aviation 2014, 20th AIAA/CEAS Aeroacoustics Conference, paper 2014-2909, Atlanta, 2014.

[9] F.C. Fuertes, E. Cecchi, J. van Beeck & C. Schram, *An inexpensive and versatile technique for wide frequency range surface pressure measurements: an application for the study of turbulent buffeting of a square cylinder*, Exp. in Fluids, 2014, 55-1627. DOI 10.1007/s00348-013-1627-y

[10] S. Moreau, J. Foss & S. Morris, *A numerical and experimental test-bed for low-speed fans*, Proc. Inst. of Mech. Eng., Part A: J. of Power and Energy, 230 (5), 2016.

[11] A. Marsan, M. Sanjosé, Y. Pasco, S. Moreau & M. Brouillette, *Unsteady Wall Pressure Measurements in an Outflow Butterfly Valve Using Remote Microphone Probes*, 22nd AIAA/CEAS Aeroacoustics Conference, AIAA paper 2016-2888, Lyon 2016.

[12] N.S. Zawodny, F.Liu & L. Cattafesta, *Transfer matrix modeling of a recessed microphone for unsteady surface pressure measurements*, Applied Acoustics 117, 2017.

[13] G. Yakhina, *Experimental study of the tonal trailing-edge noise generated by low-Reynolds number airfoils and comparison with numerical simulations*, PhD thesis Ecole Centrale de Lyon, NTT 2017LYSEC08, 2017.

[14] J. Grilliat, E. Jondeau, M. Jacob, M. Roger & R. Camussi, *Broadband noise prediction models and measurements of tip leakage flows*, 14th AIAA/CEAS Aeroacoustics Conf., paper 2008-2845, Vancouver, 2008.

[15] A.D. Pierce, *Acoustics, an Introduction to its Physical Principles and Applications*, McGraw-Hill, 1981.

[16] M. Roger & S. Pérennès, *Low-Frequency Noise Sources in Two-Dimensional High-Lift Devices*, 6th AIAA/CEAS Aeroacoustics Conference, paper 2000-1972, Lahaina, 2000.

[17] M.C. Jacob, J. Boudet, D. Casalino & M. Michard, *A rod-airfoil experiment as benchmark for broadband noise modeling*, Theor. Comput. Fluid Dynamics, 19, 171-196, 2005.

[18] Y. Rozenberg, *Modélisation analytique du bruit aérodynamique à large bande des machines tournantes : utilisation de calculs moyennés de mécanique des fluides*, thèse ECL-2007-

44, 2007.

[19] Y. Rozenberg, M. Roger & S. Moreau, *Rotating Blade Trailing-Edge Noise: Experimental Validation of Analytical Model*, AIAA J. 48(5), 2010

[20] G. M. Corcos, *Resolution of pressure in turbulence*. J. Acoust. Soc. Am., 35(2), 192–199, 1963.

[21] T.F. Brooks & T.H. Hodgson, Trailing edge noise prediction from measured surface pressures, J. Sound Vib. 78(1), 1981.

[22] B.A. Singer, Large-eddy simulation of turbulent wall-pressure fluctuations, NASA-CR 198276, 1996.

[23] B.A. Singer, Turbulent Wall-Pressure Fluctuations: New Model for Off-Axis Cross-Spectral Density, NASA-CR 198297, 1996.

[24] W.K. Blake, *Mechanics of Flow-Induced Sound and Vibration*, Academic Press 1986.

[25] M. Roger & S. Moreau, *Back-Scattering Correction and Further Extensions of Amiet's Trailing Edge Noise Model. Part1: Theory*, J. Sound Vib. vol. 286, pp. 477-506, 2005.

[26] M. Roger, *Broadband Noise from Lifting Surfaces, Analytical Modeling and Experimental Validation,* in "Noise Sources in Turbulent Shear Flows: Fundamentals and Applications", CISM Courses and Lectures vol. 545, Springer, 2013.

[27] B. M. Efimtsov, Characteristics of the field of turbulent wall pressure fluctuations at large Reynolds numbers, *Sov. Phys. Acoust.*, 28(4), 1982.

[28] C. Bonamy, *Analyse expérimentale de l'aérodynamique proche paroi et modélisation du bruit de bord de fuite d'un profil d'aile en écoulement subsonique*. Thesis Ecole Supérieure d'Ingénieurs de Poitiers - ESIP, 2007.

[29] C. Bonamy & Y. Gervais, Experimental analysis of the wall aerodynamics and acoustic radiation of the trailing edge of an airfoil in subsonic flow. Acoustics'08, Paris, 2008.

[30] G. Robert, *Environmental Noise Associated with Turbulent Boundary Layer Excitation*, ENABLE task report, GR4D-CT-2000-00223, 2002.

[31] J. S. Bendat and A. G. Piersol, *Engineering Applications of Correlations and Spectral Analysis*. John Wiley & Sons, NY, 1993.